

Modeling the dynamics of a tracer particle in an elastic active gel

E. Ben-Isaac,¹ É. Fodor,² P. Visco,² F. van Wijland,² and Nir S. Gov¹¹*Department of Chemical Physics, Weizmann Institute of Science, Rehovot 76100, Israel*²*Laboratoire Matière et Systèmes Complexes, UMR 7057 CNRS/P7, Université Paris Diderot, 10 rue Alice Domon et Léonie Duquet, 75205 Paris cedex 13, France*

(Received 18 November 2014; published 22 July 2015)

The internal dynamics of active gels both in artificial (*in vitro*) model systems and inside the cytoskeleton of living cells has been extensively studied with experiments of recent years. These dynamics are probed using tracer particles embedded in the network of biopolymers together with molecular motors, and distinct nonthermal behavior is observed. We present a theoretical model of the dynamics of a trapped active particle, which allows us to quantify the deviations from equilibrium behavior, using both analytic and numerical calculations. We map the different regimes of dynamics in this system and highlight the different manifestations of activity: breakdown of the virial theorem and equipartition, different elasticity-dependent “effective temperatures,” and distinct non-Gaussian distributions. Our results shed light on puzzling observations in active gel experiments and provide physical interpretation of existing observations, as well as predictions for future studies.

DOI: [10.1103/PhysRevE.92.012716](https://doi.org/10.1103/PhysRevE.92.012716)

PACS number(s): 87.10.Ca, 05.40.–a, 87.10.Mn

I. INTRODUCTION

In vitro experiments have probed the nonthermal (active) fluctuations in an “active gel,” which is most commonly realized as a network composed of cross-linked filaments (such as actin) and molecular motors (such as myosin-II) [1–4]. The fluctuations inside the active gel were measured using the tracking of individual tracer particles and used to demonstrate the active (nonequilibrium) nature of these systems through the breaking of the Fluctuation-Dissipation theorem (FDT) [2]. In these active gels, myosin-II molecular motors generate relative motion between the actin filaments, through consumption of ATP, and thus drive the athermal random motion of the probe particles dispersed throughout the network. This tracking technique was also implemented in living cells [5–7]. The motion of these tracers in cells was also shown to deviate from simple thermal Brownian diffusion.

There are several puzzling observations of the dynamics of the tracer particles inside the active gels, for example, the distinct non-Gaussianity of the displacement correlations and their time dependence [1,4,8]. We propose here a simple model for the random active motion of a tracer particle within a (linearly) elastic active gel, and we use our model to resolve their distinct nonequilibrium dynamics. On long time scales the tracer particles are observed to perform hopping-like diffusion, which is beyond the regime of the present model and will be treated in following work, as will be the introduction of nonlinear elasticity [9]. The activity is modeled through colored shot noise [10,11], and the elastic gel is described by a confining harmonic potential. We use the model to derive expressions directly related to the experimentally accessible observations, such as the position and velocity distributions and their deviations from the thermal Gaussian form. Our model allows us to offer a physical interpretation to existing experiments, to characterize the microscopic active processes in the active gel, and to make specific predictions for future exploration of the limits of the active forces and elasticity. The simplicity of this model makes this model applicable to a wide range of systems and allows us to gain analytic solutions, intuition, and understanding of the dynamics, which is usually

lacking in out-of-equilibrium systems. This would be more difficult to obtain with a more complex description of the gel, such as visco-elastic that has more intrinsic time scales.

II. MODEL

Our model treats a particle in a harmonic potential, kicked randomly by thermal and active forces (active noise) [11]. The corresponding Langevin equation for the particle velocity v (in one dimension or one component in higher dimensions, with the mass set to $m = 1$) is

$$\dot{v} = -\lambda v + f_a + f_T - \frac{\partial U(x)}{\partial x}, \quad (1)$$

where λ is the effective friction coefficient and the harmonic potential is $U(x) = kx^2/2$, with k proportional to the bulk modulus of the gel (related to the gel density, cross-linker density, and other structural factors). The thermal force f_T is an uncorrelated Gaussian white noise: $\langle f_T(t)f_T(t') \rangle = 2\lambda T\delta(t - t')$, with T the ambient temperature, and Boltzmann’s constant set to $k_B = 1$.

We model the active force f_a as arising from the independent action of N_m molecular motors, each motor producing pulses of a given fixed force $\pm f_0$, for a duration $\Delta\tau$ (either a constant or drawn from a Poissonian process with an average value $\Delta\tau$, i.e., shot noise), with a random direction (sign). The active pulses turn on randomly as a Poisson process with an average waiting time τ (during which the active force is zero), which determines the “duty ratio” of the motor (the probability to be turned “on”): $p_{on} = \Delta\tau/(\tau + \Delta\tau)$.

III. RESULTS: MEAN KINETIC AND POTENTIAL ENERGIES

The mean-square velocity and position fluctuations of the trapped particle, essentially the mean kinetic ($T_v = \langle v^2 \rangle$) and potential ($T_x = k\langle x^2 \rangle$) energies, can be calculated for the case of shot noise force correlations [details given in the Appendices, Eqs. (A1a)–(C4), and Figs. 3–4]. Note that the mean $\langle \cdot \rangle$ is over many realizations of the system or over a long

time. In the limit of vanishing trapping potential the position fluctuations $\langle x^2 \rangle$ diverge, but the potential energy approaches a constant: $T_x|_{k \rightarrow 0} \rightarrow f_0^2 \Delta\tau/\lambda$. The kinetic energy approaches the constant value for a free particle [11]: $T_v|_{k \rightarrow 0} \rightarrow T_x/(1 + \lambda\Delta\tau)$. We therefore find that the virial theorem is in general not satisfied in this active system, which in a harmonic potential gives $T_v|_{eq} = T_x|_{eq}$, even in the limit of weak trapping. The virial theorem, and equipartition, breaks down due to the strong correlations between the particle position and the applied active force: In the limit of perfect correlations, the particle is stationary at $x = \pm x_0$ when the force is turned on (the stationary position in the trap where the potential balances the active force: $x_0 = f_0/k$), and at $x = 0$ when it is off. In this extreme case the potential energy is finite while the kinetic energy is zero.

In the limit of strong trapping $k \rightarrow \infty, k/\lambda^2 \gg 1$, the potential energy behaves as $T_x \propto k^{-1}$ [Eqs. (B6) and (B9)], while the kinetic energy decays faster as $T_v \propto k^{-3/2}$ [Eq. (D2)]. One can understand this limit as follows: When the trapping is very strong, the shortest time scale in the problem is the natural oscillation frequency in the trap, $\omega_k \sim \sqrt{k}$. In this regime of $k\Delta\tau^2 \gg 1$ we find that during the active pulse $\Delta\tau$, the particle reaches x_0 , and the mean potential energy is therefore proportional to $T_x \sim kx_0^2 \propto 1/k$. The kinetic energy in this limit decays faster, since the fraction of time that the particle is moving is only during the acceleration phase determined by the time scale $\omega_k^{-1} \sim \sqrt{k}$. We therefore find that in the presence of strong elastic restoring forces the potential energy will be much larger than the kinetic energy, in an active system ($T_x \gg T_v$). This was recently found in the study of active semiflexible polymers [12].

Note that in a real active gel the different parameters maybe coupled: larger local density of the network filaments increases the local value of the elastic stiffness parameter k but may also increase locally the density of motors and their ability to exert an effective force, thereby increasing N_m and f_0 . The tracer bead behavior as expressed by T_v and T_x can therefore be a complex function of the local network parameters.

IV. RESULTS: VELOCITY AND POSITION DISTRIBUTIONS

The distributions of the velocity and position in the different regimes are shown in Fig. 1 for the case of a single active motor. The simulations of the model were carried out using explicit Euler integration of Eq. (1) (see also the Appendices for details). We study this case in order to highlight the deviations from Gaussian (equilibrium-like) behavior, which is restored by many simultaneous motors [11]. In an infinite gel, with a constant density of motors, we may therefore treat the distant (and numerous) motors as giving rise to an additional thermal-like contribution to the tracer dynamics [Eqs. (D1) and (D2)], while the nonequilibrium behavior is dominated by a single proximal motor [1].

In the limit of weak damping, $\lambda\Delta\tau \ll 1$, both the position and velocity distributions are very close to Gaussian, with the width of the Gaussian distributions given by T_v and T_x [Figs. 1(b) and 1(d), Eqs. (B4) and (C1)]: $P(v) \propto \exp[-v^2/(2T_v)]$, $P(x) \propto \exp[-kx^2/(2T_x)]$.

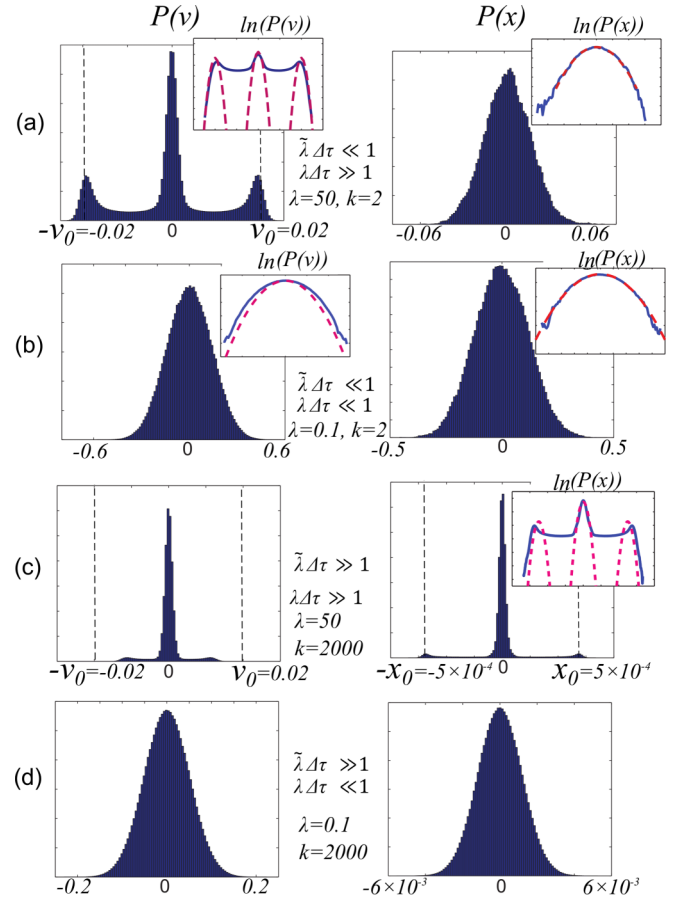


FIG. 1. (Color online) Distribution of position and velocity for particle trapped within a harmonic trap of various stiffness ($k = 1, 1000$ for a, b and c, d, respectively) and for different regimes of friction ($\lambda = 50, 0.1$ for a, c and b, d, respectively). The time scale of the active bursts is $\Delta\tau = 0.1$, the amplitude of the active force $f_0 = 1$, and the waiting time $\tau = 1$ (so that $p_{on} \approx 0.1$). For simplicity we plot the behavior for the case of a single motor with a constant burst duration. The insets compare the simulated distribution (blue line) to the analytic approximation (red dashed line), in log-linear scale, as simple Gaussians or as a sum of shifted thermal Gaussians.

In the highly damped limit, $\lambda\Delta\tau \gg 1$, the distributions become highly non-Gaussian [Figs. 1(a) and 1(c)]. We can make a useful approximation in this limit, by neglecting the inertial term in Eq. (1) and get the following equation for the particle position x inside the potential well:

$$\lambda v = -kx + f_a + f_T \quad (2)$$

$$\Rightarrow \dot{x} = -\tilde{\lambda}x + \frac{f_a + f_T}{\lambda}, \quad (3)$$

where $\tilde{\lambda} = k/\lambda$. This equation is now analogous to the equation for the velocity v of a free particle [Eq. (1) when $U(x) = 0$]. Due to this analogy we can use the analytic solutions for the free particle [11] to describe the particle position in the well. For weak trapping [Fig. 1(a)], we therefore expect the position distribution to be roughly Gaussian, since we are in the limit of $\tilde{\lambda}\Delta\tau \ll 1$ of Eq. (3), with a width given by [from

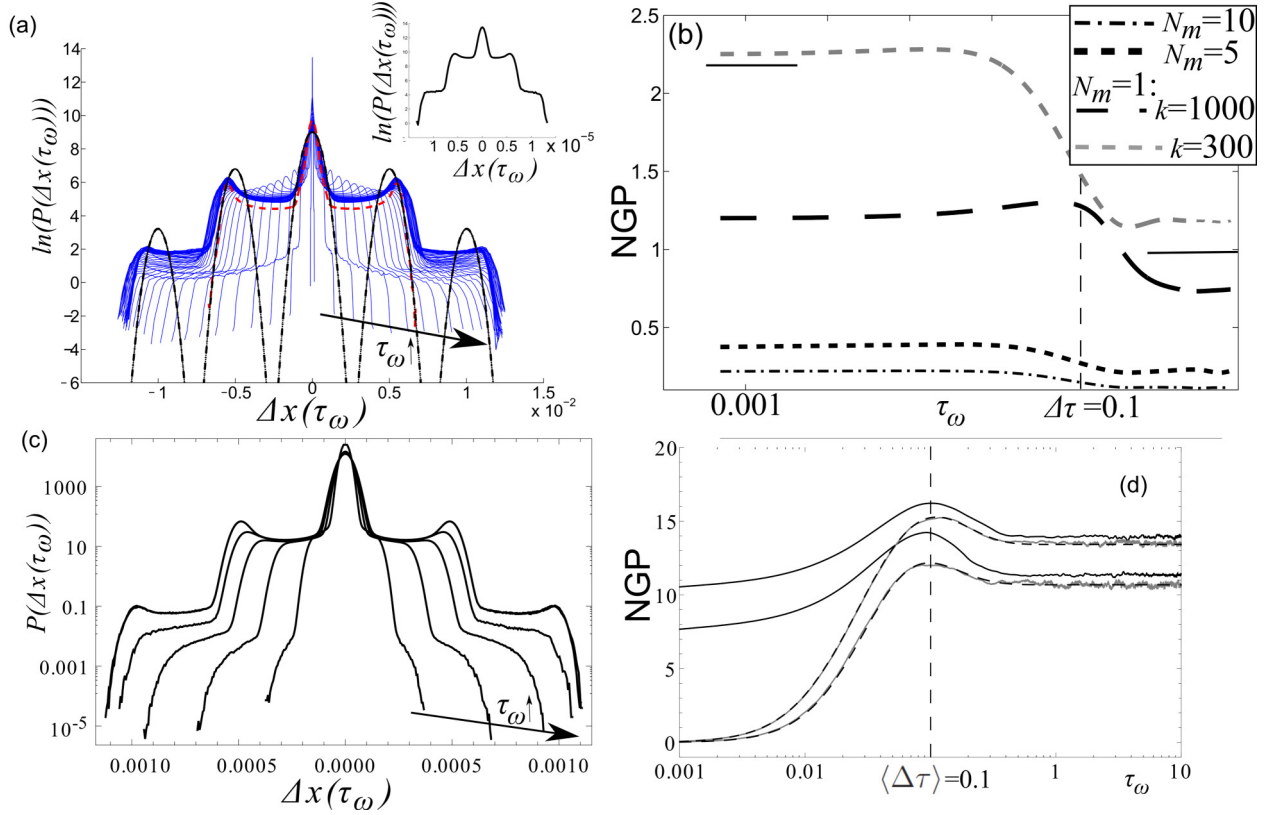


FIG. 2. (Color online) (a) Distribution of particle displacements $P[\Delta x(\tau_\omega)]$, for various lag time duration τ_ω (blue lines), for a single motor and constant burst duration. The traces correspond to increasing time lag durations (black arrow), in the range $1 > \tau_\omega > 5 \times 10^{-4}$. The red dashed line denotes the spatial distribution $P(x)$, and the black dashed lines denote $P[\Delta x(\infty)]$ [Eq. (6)] for the approximation of $P(x)$ as a sum of three Gaussians. Inset shows the displacement distribution for very short lag times τ_ω . Parameters as in Fig. 1(c). (b) Calculated NGP for the $P[\Delta x(\tau_\omega)]$, for various number of motors (N_m), and confinement strength. The short horizontal black lines denote (left) the NGP of $P(x)$, and (right) of $P[\Delta x(\infty)]$ [Eq. (6)], for the $k = 1000, N_m = 1$ case. (c) Displacement distributions [as in (a)] for a calculation without the inertia term [Eq. (2)], using $k = 1000$, Poissonian $\langle \Delta \tau \rangle = 0.1$, and increasing lag time indicated by the arrow $\tau_\omega = 10^{-3}, 2.5 \times 10^{-3}, 5 \times 10^{-3}, 10^{-2}, 1$, and (d) the corresponding NGP, comparing the simulation (solid gray lines) to the analytical result (see Appendix for details, dashed lines), for $k = 300, 1000$ (top, bottom). The NGP with inertia is given by the solid black lines.

Eq. (3) and (B6)]

$$T'_x = \frac{p_{on} N_m \lambda (\tilde{\lambda} \Delta \tau + e^{-\tilde{\lambda} \Delta \tau} - 1)}{k^2 \Delta \tau} f_0^2, \quad (4)$$

$$T_x = 2 \frac{p_{on} N_m \langle \Delta \tau \rangle}{\lambda (1 + \tilde{\lambda} \langle \Delta \tau \rangle)} f_0^2, \quad (5)$$

where T'_x describes the case of a constant $\Delta \tau$ and T_x the case of a Poissonian burst distribution and fits well the calculated distribution [inset of Fig. 1(a)]. In the limit of weak confinement we expect the velocity distribution to approach the behavior of the free damped particle [11], which is well approximated as a sum of thermal Gaussians, centered at $v = 0, \pm v_0$ ($v_0 = F_0/\lambda$). This is indeed a good approximation, as shown in the inset of Fig. 1(a).

For strong potentials [$\tilde{\lambda} \Delta \tau \gg 1$, Fig. 1(c)] we expect from the analogy given in Eq. (3) that the spatial distribution is now well described by the sum of shifted thermal Gaussians [Fig. 1(c)] [11], centered at $x = 0, \pm x_0$. The velocity distribution in this regime is also non-Gaussian: the maximal active velocity is of order v_0 at the origin of the potential, but since the particle immediately slows due to the confinement (up to a

complete stop at $\pm x_0$), the peaks of the distribution are located at roughly $\pm v_0/2$.

V. RESULTS: NON-GAUSSIANITY OF THE DISPLACEMENT DISTRIBUTION

The distribution of relative particle displacements (Van Hove correlation function) $P[\Delta x(\tau_\omega)]$, where $\Delta x(\tau_\omega) = x(t + \tau_\omega) - x(t)$ (τ_ω is the lag-time duration), is a useful measure for the particle dynamics. We plot it in Fig. 2(a) for the interesting regime of strong confinement and damping and compared to the distribution of particle positions $P(x)$ [Fig. 1(c)]. We see that $P[\Delta x(\tau_\omega)]$ has double the number of peaks of $P(x)$ and is distinctly non-Gaussian for all τ_ω . In Fig. 2(c) we show that the same qualitative behavior is obtained for Poissonian burst duration.

The deviations from Gaussianity are quantified in Fig. 2(b) using the Non-Gaussianity Parameter (NGP) of the displacement distributions: $\kappa = \langle \Delta x^4 \rangle / 3 \langle \Delta x^2 \rangle^2 - 1$. This deviation of the kurtosis from the value for a Gaussian is an established measure for studying distributions [13]. We find that the NGP has a finite value for $\tau_\omega \rightarrow 0$. This is as a consequence of the periods during which the particle is accelerated by the active

force, and the result is a finite probability for displacements of the order of $\Delta x \simeq v_0 \tau_\omega$ [inset of Fig. 2(a)]. With increasing τ_ω the NGP reaches a maximum, at lag times that are of order $\Delta \tau$, where the full effect of the active bursts is observed.

We find that the maximal value of the NGP for $P[\Delta x(\tau_\omega)]$ is close to the NGP of $P(x)$ [Fig. 2(b)], which is a function for which we have a good analytic approximation [11] [Eqs. (F1) and (F2)]. In the limit of $\tau_\omega \rightarrow \infty$ the calculated NGP remains finite and can be calculated analytically since the displacement distribution becomes

$$P[\Delta x(\infty)] = \int_{-\infty}^{\infty} P(x)P(x + \Delta x) dx, \quad (6)$$

and the $P(x)$ in this regime is well approximated by the sum of shifted thermal Gaussians [inset of Fig. 1(c)]. This calculation fits well the simulated result [Fig. 2(b)]. For a larger number of motors, the distribution $P[\Delta x(\tau_\omega)]$ approach a Gaussian [Figs. 2(b) and 6)].

In the limit where we discard inertia from the equations of motion [Eq. (2)], we can calculate the NGP analytically (see details in the Appendices). In Fig. 2(c) we plot the displacement distributions for this case, and in Fig. 2(d) we show that indeed the analytical calculation describes exactly the simulation results. We find that this treatment captures correctly the qualitative features of the full system, such as the position of the peak, followed by a constant value at long lag times. The large discrepancy is in the limit of $\tau_\omega \rightarrow 0$, where the inertial effects of the oscillations inside the trap are missing from Eq. (2).

VI. RESULTS: FDT

An alternative method to characterize the nonequilibrium dynamics is through the deviations from the FDT [2]. We can quantify these deviations by defining an effective temperature, using the Fourier transform of the position fluctuations $[S_{xx}(\omega)]$ and linear response [susceptibility of the position to an external force $\chi(\omega)]$ of the system. We can calculate both for our trapped particle position using Eq. (3) for the $\tilde{\lambda} \Delta \tau \gg 1$ limit, to get [for Poissonian burst duration $\Delta \tau$, see details in Appendix G, Eqs. (G1)–(G3)]

$$T_{FDT}(\omega) = \frac{\omega S_{xx}(\omega)}{2\text{Im}[\chi(\omega)]} = \frac{N_m p_{on} f_0^2 \langle \Delta \tau \rangle}{\lambda [1 + (\omega \langle \Delta \tau \rangle)^2]} + T. \quad (7)$$

Note that $T_{FDT}(\omega)$ is independent of the shape of the harmonic potential (k) and is identical to the result for a free active particle [11]. This result highlights the fact that while different “effective temperatures” in an active system [T_v and T_x , Eqs. (4) and (5)] give a measure of the activity, they can have very different properties.

VII. DISCUSSION

We now use our results to interpret several experiments on active gels *in vitro* and extract the values that characterize these active systems. In Ref. [2] the breakdown of the FDT was measured. Comparing to our T_{FDT} [Eq. (G3)] we find that the onset of the deviation from equilibrium occurs for frequencies $\omega \leq \Delta \tau^{-1}$, from which we find that $\Delta \tau \approx 100$ ms, which is the scale of the release time of the myosin-II-induced stress [2] in this system. The measured deviation from

the FDT was found to increase with decreasing frequency [2] and at the lowest measured frequencies the ratio was found to be $T_{FDT}(\omega \rightarrow 0)/T \approx 20\text{--}100$. This number fixes for us the combination of the parameters given in Eq. (G3).

Recent experiments shed more detail on the active motion in this system [1], and it was found that the tracer particle performs random confined motion interspersed by periods of large excursions. The confined motion part can be directly related to the mean-square displacement in our model T_x [Eq. (5)] and is observed to be a factor of $T_x/T \approx 10\text{--}50$ larger than in the inert system (not containing myosins) [1]. These values are in general agreement with the values extracted above for T_{FDT} from Ref. [2], and note that we predict [Eqs. (5) and (G3)]: $T_{FDT}(\omega \rightarrow 0)/T_x = 1 + \tilde{\lambda} \langle \Delta \tau \rangle > 1$.

Furthermore, in these experiments [1] it was observed that the distribution of relative particle displacements $P[\Delta x(\tau_\omega)]$ is highly non-Gaussian. Comparing this to Fig. 2(b) we note that both the experiments and in our calculations the NGP has a finite value for $\tau_\omega \rightarrow 0$. With increasing τ_ω the NGP reaches a maximum, both in the experiments and in our calculations [Figs. 2(b) and 2(d)]. By comparing to our model we expect the peak to appear at $\tau_\omega \approx \Delta \tau$, so the observations [1] suggest the burst duration is of order $\Delta \tau \approx 1\text{--}10$, in agreement with similar studies [4,8]. Note that very similar NGP time scales were observed in living cells [14,15] Our model predicts that the maximal value of the NGP is a nonmonotonous function of p_{on} , and this may be explored by varying the concentration of ATP in the system. Furthermore, from our model we predict that the NGP decrease with decreasing active force, and increasing stiffness of the confining network [Figs. 2(b) and 2(d), Eq. (F2)]. These predictions can be related to the observed activity dependence of the NGP in cells [15] and the decay of the NGP during the aging and coarsening of an active gel [4].

The large observed deviations from Gaussianity indicate that the particle is in the strong confinement regime: $\tilde{\lambda} \langle \Delta \tau \rangle > 1$. The maximal value of the observed NGP $\approx 2\text{--}4$ can be used to get an estimate of T_x , by taking it to be equal to NGP_{\max} [Eq. (F2)]. This gives us $T_x \approx 10\text{--}30 k_B T$ and $p_{on} \approx 2\%\text{--}3\%$. This value of T_x is in good agreement with the estimate made above. The value of p_{on} is in agreement with the observation that the waiting-time between bursts is much longer than the burst duration [2], and with the measured duty ratio of myosin-II [16].

In the limit of $\tau_\omega \rightarrow \infty$ the observed NGP of the displacement distribution $P[\Delta x(\tau_\omega)]$ decays to zero [1], while for the calculated confined particle the NGP remains finite [Figs. 2(b) and 2(d)]. At long times ($\gtrsim 10$ s) the observed trajectory has large excursions [1], which we interpret as the escape of the particle from the confining potential. The ensuing hopping-type diffusion causes the NGP to vanish, as for free diffusion [17]. Within our model we therefore interpret the observed time scale of the vanishing of the NGP, $\tau_\omega \approx 10\text{--}100$ s, as the time scale, which corresponds to the mean trapping time of the bead within the confining actin gel. Beyond this time scale the bead has a large chance to escape the confinement, and hop to a new trapping site, which corresponds to a reorganization of the actin network. The real actin-myosin gel undergoes irreversible processes that make its properties time-dependent and render it inhomogeneous [4,18–20]. Such effects make the comparison to the model

much more challenging. Large deviations from Gaussianity were also observed for the Van Hove correlations in other forms of active gels [21].

VIII. CONCLUSION

We investigated here the dynamics of a trapped active particle, with several interesting results: (i) The activity leads to strong deviations from equilibrium, such as the breakdown of the virial theorem and equipartition. We find that in the presence of elastic restoring forces the activity is mostly “stored” in the potential energy of the system. (ii) Different “effective temperatures” give a measure of the activity, and some are dependent on the stiffness of the elastic confinement. (iii) The displacement, position, and velocity distributions of the particle are highly non-Gaussian in the regime of strong elastic confinement and small number of dominant motors. These distributions can be used, together with our simple model, to extract information about the microscopic properties of the active motors. Note that in our model the activity affects the motion and position distributions of the trapped particle, which is complementary to models where the activity drives only the large-scale reorganization that moves the particle between trapping sites [22,23] or leads to network collapse [24]. The results of this model are in good agreement with observations of the dynamics of tracer beads inside active gels, and the simplicity of the model may make it applicable for a wide range of systems. More complex viscoelastic relations can be used in place of the simple elasticity presented here to describe the dynamics inside living cells [25,26], as well as nonlinear elasticity [9]. Note that in most current experiments on actin-myosin gels, the myosin-driven activity is strong enough to lead to large-scale reorganization of the actin network, eventually leading to the network collapse [4,18–20]. In order to observe the active motion for the elastically trapped tracer in the intact network, which we have calculated, much weaker active forces will be needed. Our work can therefore give motivation for such future studied.

ACKNOWLEDGMENTS

N.S.G. would like to thank ISF Grant No. 580/12 for support. This research is made possible in part by the historic generosity of the Harold Perlman Family.

APPENDIX A: NUMERICAL SIMULATIONS

The simulations of the dynamics of the particle inside the one-dimensional harmonic potential were carried out using explicit Euler integration of Eq. (1). We were careful to use a small time step Δt , such that it was always an order of magnitude smaller than the smallest time scale in the problem. The time scales in the problem are $\tau, \Delta\tau$ and $\sqrt{2/k}$, where the last time scale is that of the oscillation frequency of the particle inside the harmonic potential.

The iterative equations take the following form in terms of the sampling time Δt :

$$v(t + \Delta t) = v(t) + [-\lambda v(t) - kx(t) + f_a(t)]\Delta t + \sqrt{2\lambda T \Delta t} \eta, \quad (\text{A1a})$$

$$x(t + \Delta t) = x(t) + v(t)\Delta t, \quad (\text{A1b})$$

where η is a random Gaussian variable with zero mean and variance 1. Considering that both the waiting time and the persistence time are exponentially distributed with mean values τ and $\Delta\tau$, respectively, the iterative equation for the active force f_a obeys

$$f_a(t + \Delta t) = \begin{cases} f_a(t) & \text{if } f_a(t) \neq 0 & \text{prob. } 1 - \Delta t / \Delta\tau, \\ f_a(t) & \text{if } f_a(t) = 0 & \text{prob. } 1 - \Delta t / \tau, \\ 0 & \text{if } f_a(t) \neq 0 & \text{prob. } \Delta t / \Delta\tau, \\ \epsilon_{\{-f, f\}} & \text{if } f_a(t) = 0 & \text{prob. } \Delta t / \tau, \end{cases} \quad (\text{A2})$$

where $\epsilon_{\{-f, f\}} = \{f, -f\}$ with same probability.

APPENDIX B: POSITION FLUCTUATIONS OF A TRAPPED PARTICLE

From the model equations of motion [Eq. (1)], we can calculate the mean-square fluctuations in the particle position for a shot noise force correlations with average burst duration $\Delta\tau$. We begin by Fourier transforming Eq. (1) to get

$$-\omega^2 \tilde{x} = i\omega\lambda \tilde{x} + \tilde{f}_a + \tilde{f}_T - k\tilde{x}, \quad (\text{B1})$$

where the $\tilde{}$ denotes the FT. From Eq. (B1) we get

$$\tilde{x}(\omega) = \frac{\tilde{f}_a(\omega) + \tilde{f}_T(\omega)}{-\omega^2 - i\omega\lambda + k}. \quad (\text{B2})$$

The fluctuations (correlations) are therefore

$$\langle x^2 \rangle(\omega) = \langle \tilde{x}(\omega) \tilde{x}^*(\omega) \rangle = \frac{\langle \tilde{f}_a^2 \rangle(\omega) + \langle \tilde{f}_T^2 \rangle(\omega)}{(k - \omega^2)^2 + (\omega\lambda)^2}, \quad (\text{B3})$$

where we have $\langle \tilde{f}_a^2 \rangle(\omega) = N_m P_{on} f_0^2 \frac{\Delta\tau}{1 + (\omega\Delta\tau)^2}$ (Poissonian shot noise with mean burst length $\Delta\tau$), and $\langle \tilde{f}_T^2 \rangle(\omega) = 2\lambda T$ (thermal white noise) [11].

For the active part alone, we get

$$\langle x^2 \rangle = \frac{N_m P_{on} f_0^2}{2\pi} \int_0^\infty \frac{1}{(\omega^2 - k)^2 + (\omega\lambda)^2} \frac{\Delta\tau}{1 + (\omega\Delta\tau)^2} d\omega. \quad (\text{B4})$$

The solution for this integral is quite lengthy. In the limit of weak trapping, $k \rightarrow 0$, we get that the mean-square displacement diverges,

$$\langle x^2 \rangle \rightarrow 2 \frac{N_m P_{on} f_0^2 \Delta\tau}{k(k\Delta\tau + \lambda)}, \quad (\text{B5})$$

such that the mean potential energy in this limit approaches a constant value

$$T'_x \simeq k \langle x^2 \rangle \rightarrow 2 \frac{N_m P_{on} f_0^2 \Delta\tau}{(k\Delta\tau + \lambda)}. \quad (\text{B6})$$

In the limit of large k , we can expand the integrand of Eq. (B4) in powers of k^{-1} to get the integral

$$\langle x^2 \rangle = \frac{2N_m P_{on} f_0^2}{\pi} \int_0^{\sqrt{k}} \frac{\Delta\tau}{k^2 [1 + (\omega\Delta\tau)^2]} d\omega, \quad (\text{B7})$$

which is also bound with a maximal frequency corresponding to the natural frequency of the harmonic trap. This integral gives a simple expression, which gives a good fit description

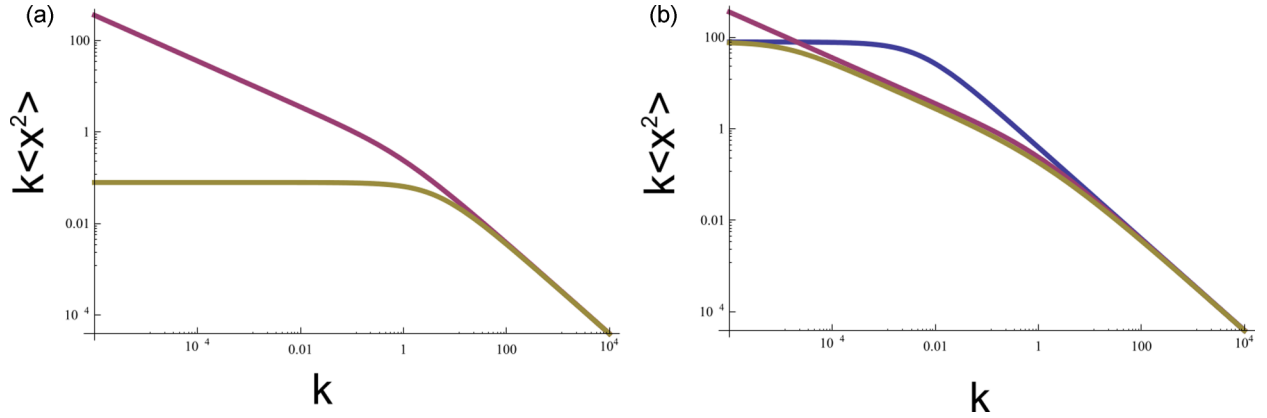


FIG. 3. (Color online) Calculated mean-square position fluctuations (plotted as a mean potential energy) for the trapped particle: Brown line, full solution; purple line, approximate solution [Eq. (B8)]; blue line, approximate expression T'_x for the limit $\lambda\Delta\tau \gg 1$ [Eq. (B9)]. In both panels we used $\Delta\tau = 1$, and (a) $\lambda = 10$, (b) $\lambda = 0.01$. In (a) the blue line agrees perfectly with the full solution, while in (b) it has a discrepancy at intermediate confinements.

as long as $k \gg \lambda^2$ (Fig. 3):

$$\langle x^2 \rangle_k = \frac{2N_m p_{on} f_0^2}{\pi k^2} \arctan[\sqrt{k/2}\Delta\tau]. \quad (\text{B8})$$

Finding the value of k for which the scaling changes from $\langle x^2 \rangle \sim k^{-3/2}$ to $\langle x^2 \rangle \sim k^{-2}$, is simply by equating the large and small k limits of $\langle x^2 \rangle_k$ [Eq. (B8)].

In the limit of $\lambda\Delta\tau \gg 1$ we find the simple approximate expression (Fig. 3)

$$T'_x \simeq k \langle x^2 \rangle \simeq \frac{\Delta\tau N_m p_{on} f_0^2}{8\lambda^2(k\Delta\tau/2\lambda + 1)}. \quad (\text{B9})$$

The numerical simulations, in the highly damped limit ($\lambda\Delta\tau \gg 1$) indicate the k^{-1} and k^{-2} limits [Fig. 4(a)].

APPENDIX C: VELOCITY FLUCTUATIONS OF A TRAPPED PARTICLE

Similar to the procedure for the position fluctuations described above, we can calculate the velocity fluctuations. The mean-square fluctuations in the particle velocity are given

simply from Eq. (B4) by

$$\langle v^2 \rangle = \frac{N_m p_{on} f_0^2}{2\pi} \int_0^\infty \frac{\omega^2}{(\omega^2 - k)^2 + (\omega\lambda)^2} \frac{\Delta\tau}{1 + (\omega\Delta\tau)^2} d\omega. \quad (\text{C1})$$

The solution for this integral is again quite lengthy. As for the position distribution, we can find an approximation for the large k limit, using

$$\langle v^2 \rangle = \frac{2N_m p_{on} f_0^2}{\pi} \int_0^{\sqrt{k}} \frac{\omega^2 \Delta\tau}{k^2 [1 + (\omega\Delta\tau)^2]} d\omega, \quad (\text{C2})$$

which is also bound with a maximal frequency corresponding to the natural frequency of the harmonic trap. This integral gives a simple expression, which gives a good fit description as long as $k \gg \lambda^2$:

$$\langle v^2 \rangle_k = \frac{2N_m p_{on} f_0^2}{\pi k^2 \Delta\tau^2} (\sqrt{k/2}\Delta\tau - \arctan[\sqrt{k/2}\Delta\tau]). \quad (\text{C3})$$

The scaling of $\langle v^2 \rangle_k$ changes from $\langle v^2 \rangle \sim k^{-0.5}$ to $\langle v^2 \rangle \sim k^{-3/2}$ as k increases [Fig. 5(b)].

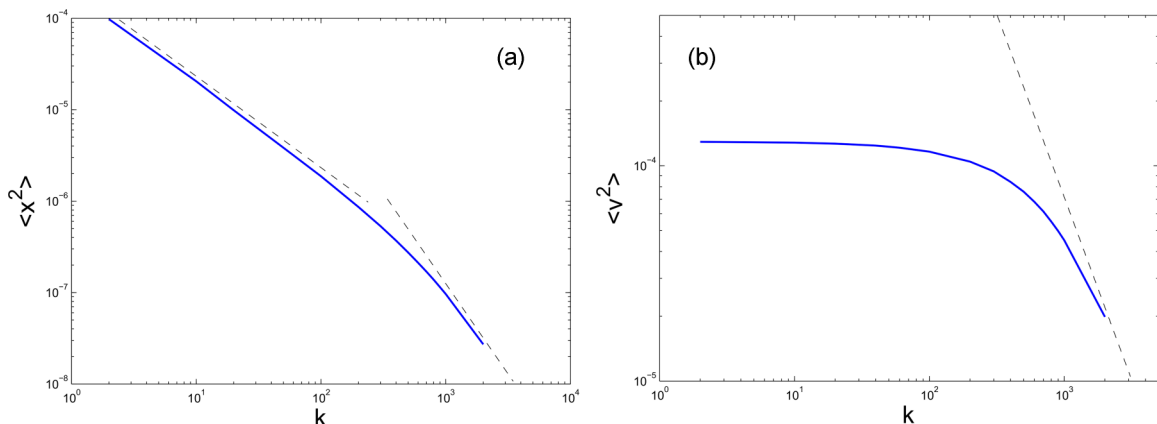


FIG. 4. (Color online) Simulated mean-square particle displacements (a) and velocity (b) in the limit of $\lambda\Delta\tau \gg 1$, using $\Delta\tau = 1$, $\lambda = 50$, $f_0 = 1$, $p_{on} = 0.1$. The dashed lines indicate the power laws with exponents -1 , -2 in (a) and $-3/2$ in (b).

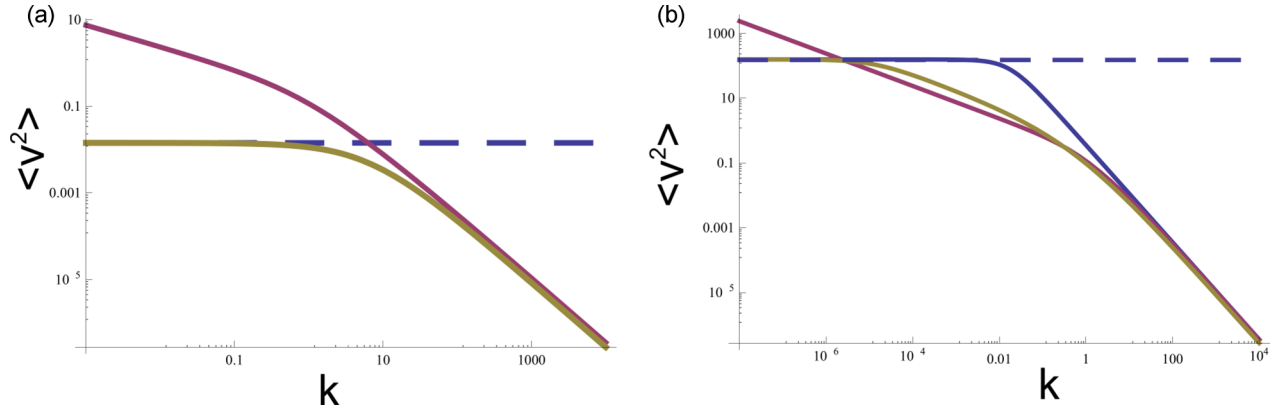


FIG. 5. (Color online) Calculated mean-square velocity fluctuations for the trapped particle: brown line, full solution; purple line, approximate solution [Eq. (C3)]; blue line, highly damped limit [Eq. (C4)]; and the dashed blue line is the free-particle value [11]. In both panels we used $\Delta\tau = 1$ and (a) $\lambda = 10$, (b) $\lambda = 0.01$.

In the limit of $\lambda\Delta\tau \gg 1$ we have the simple approximate expression

$$\langle v^2 \rangle \simeq \frac{\Delta\tau N_m p_{on} f_0^2}{4[\lambda(1 + \Delta\tau\lambda) + \pi\Delta\tau^2\sqrt{k^3/8}]}, \quad (\text{C4})$$

which fits quite well the full expression in Fig. 5(a).

The numerical simulations, in the highly damped limit ($\lambda\Delta\tau \gg 1$) indicate the k^0 and $k^{-3/2}$ limits [Fig. 4(b)].

APPENDIX D: EFFECTIVE TEMPERATURE DUE TO FORCES FROM DISTANT (AND NUMEROUS) MOTORS

In a linear elastic medium, the displacements and stresses decay from a point source (at least) as $1/r^2$. Since there are numerous distant motors affecting the bead, their cumulative random forces are most likely to give rise to Gaussian distribution of position and velocities for the trapped particle. Each shell (of thickness dr) at radius r from the tracer beads has $N_m(r) = 4\pi r^2 \rho dr$ motors (at constant density ρ), and therefore they contribute to the mean-square velocity the following contribution [in the limit of $\lambda\Delta\tau \gg 1$, using Eq. (C4)]:

$$\begin{aligned} \langle v^2 \rangle &\simeq N_m(r) \left(N_m p_{on} f_0 \frac{a^2}{r^2} \right)^2 \frac{\Delta\tau}{4[\lambda(1 + \Delta\tau\lambda) + \pi\Delta\tau^2\sqrt{k^3}]} \\ &\propto \frac{1}{r^2}, \end{aligned} \quad (\text{D1})$$

where we isolated the number of motors and the r dependence of the active forces and introduced a length scale a beyond which the far-field calculation holds. Integrating this expression we get

$$\langle v^2 \rangle_{far} \simeq \langle v^2 \rangle_0 (4\pi\rho a^3), \quad (\text{D2})$$

where $\langle v^2 \rangle_0$ is the value for the single proximal motor given in Eq. (C4). We find that the far-field contribution of the distant motors is proportional to their density ρ .

APPENDIX E: DISPLACEMENT DISTRIBUTION FOR NUMEROUS MOTORS

As the number of motors kicking the particle (N_m) increases, we find that the distribution of the particle position becomes more Gaussian, even in the limit of larger damping $\lambda\Delta\tau \gg 1$ and strong confinement $\tilde{\lambda}\Delta\tau \gg 1$. We demonstrate this in Fig. 6, which shows that the position distributions $P(x)$ and the displacement distributions $P[\Delta x(\tau_\omega)]$ approach a Gaussian for N_m larger than ~ 10 .

APPENDIX F: NGP FOR THE HIGHLY DAMPED LIMIT

We find that the maximal value of the NGP for $P[\Delta x(\tau_\omega)]$ is close to the NGP of $P(x)$ [Fig. 2(b)], which is a function for which we have a good analytic approximation [11], given by

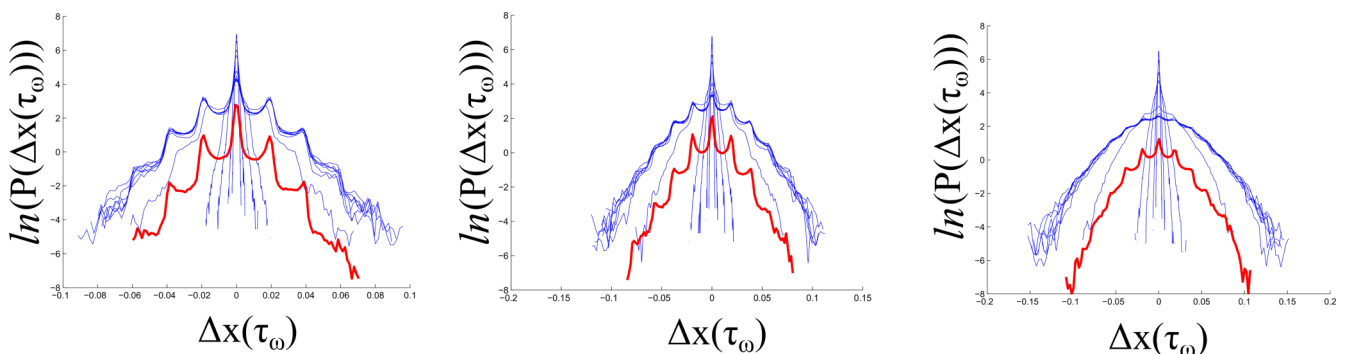


FIG. 6. (Color online) Simulated particle position distribution $P(x)$ (red lines) and displacement distributions $P(\Delta x(\tau_\omega))$ (blue lines), for increasing number of motors: $N_m = 5, 10, 20$ (left to right), using $\Delta\tau = 1$, $\lambda = 50$, $f_0 = 1$, $p_{on} = 0.1$.

(for a single motor)

$$NGP(N_m = 1) = \frac{4(1 - 3p_{on})p_{on}^3 T_{x,1}^2}{3(1 + 2p_{on}^2 T_{x,1})^2}, \quad (\text{F1})$$

where $T_{x,1}$ is the effective temperature of the spatial distribution [Eqs. (4) and (5)] for $p_{on} = 1$. The maximal value of the NGP for a single motor, as a function of p_{on} is obtained from Eq. (F1) at $p_{on} = \alpha/(2 + 6\alpha)$ and is given by

$$NGP_{\max} = \frac{(1 + 3\alpha)^2}{3\alpha(2 + 3\alpha)} - 1, \quad (\text{F2})$$

where $\alpha = k_B T / T_{x,1}$. This is a monotonously decreasing function of the stiffness k , due to the decrease in $T_{x,1}$ in stiffer gels [Eqs. (4) and (5)].

APPENDIX G: EFFECTIVE TEMPERATURE FROM THE FDT, T_{FDT}

Following Ref. [11], and using Eq. (3), we can write for the $\tilde{\lambda}\Delta\tau \gg 1$ limit (when $T = 0$)

$$\text{Response : } \chi_{xx}(\omega) = \frac{1}{\gamma(i\omega - \tilde{\lambda})}, \quad (\text{G1})$$

$$\text{Fluctuations : } S_{xx}(\omega) = \frac{f_0^2}{\lambda(\tilde{\lambda}^2 + \omega^2)} \frac{\langle \Delta\tau \rangle}{1 + (\omega\langle \Delta\tau \rangle)^2}, \quad (\text{G2})$$

$$\Rightarrow T_{FDT}(\omega) = \frac{\omega S_{xx}(\omega)}{2\text{Im}[\chi(\omega)]} = \frac{N_m p_{on} f_0^2 \langle \Delta\tau \rangle}{\lambda[1 + (\omega\langle \Delta\tau \rangle)^2]}, \quad (\text{G3})$$

resulting in Eq. (G3).

APPENDIX H: ANALYTIC CALCULATION OF THE NGP WITHOUT INERTIAS

To compute the expression of the NGP, we derive the mean quartic displacement (MQD) $\langle \Delta x^4 \rangle$ in the regime where it is

time translational invariant:

$$\langle \Delta x^4 \rangle = \langle \Delta x_T^4 \rangle + \langle \Delta x_A^4 \rangle + 6\langle \Delta x_T^2 \rangle \langle \Delta x_A^2 \rangle, \quad (\text{H1})$$

where the subscripts T and A refer, respectively, to the thermal and active contributions. The expression of the MSD is given by

$$\begin{aligned} \langle \Delta x_T^2 \rangle(t) &= \frac{2k_B T}{k} (1 - e^{-t/\tau_r}), \\ \langle \Delta x_A^2 \rangle(t) &= \frac{2k_B T_A/k}{(\tau/\tau_r)^2 - 1} \left[\frac{\tau}{\tau_r} (1 - e^{-t/\tau}) + e^{-t/\tau_r} - 1 \right], \end{aligned} \quad (\text{H2})$$

where $\tau_r = \lambda/k$ is a thermal relaxation time scale. The MQD under purely thermal conditions is related to the thermal MSD since the thermal process is Gaussian $\langle \Delta x_T^4 \rangle = 3\langle \Delta x_T^2 \rangle^2$. To compute the active MQD, we separate the position displacement $\Delta x_A(t_i, t_f) = x_A(t_f) - x_A(t_i)$ in several contributions, such that $\langle \Delta x_A^4 \rangle$ is a power law combination of these contributions. We compute each term using the active force statistics and take the limit of large t_i at fixed t corresponding to the time translational regime. The advantage of the separation we propose is that each term of the active MQD converges in such limit. The appropriate separation is

$$\Delta x_{A,a}(t_i, t_f) = (e^{-t/\tau_r} - 1) \int^{t_i} dt' \chi(t_i - t') f_A(t'), \quad (\text{H3a})$$

$$\Delta x_{A,b}(t_i, t_f) = \int^t dt' \chi(t - t') f_A(t_i + t'), \quad (\text{H3b})$$

where $\chi(t) = e^{-t/\tau_r}/\lambda$ is the noncausal response function, and $t = t_f - t_i$ is the time lag. In the time translational regime, we compute

$$\langle \Delta x_{A,a}^4 \rangle(t) = T_A^2 \frac{3\tau_r^4 (2\tau_0 + \tau_r)(\tau_0 + \tau) e^{-\frac{4t}{\tau_r}} (e^{t/\tau_r} - 1)^4}{\lambda^2 (\tau_r + \tau)(\tau_r + 3\tau)[\tau_r(\tau_0 + \tau) + 2\tau_0\tau]}, \quad (\text{H4a})$$

$$\langle \Delta x_{A,a}^3 \Delta x_{A,b} \rangle(t) = T_A^2 \frac{3\tau_r^4 \tau (2\tau_0 + \tau_r)(\tau_0 + \tau) e^{-\frac{4t}{\tau_r}} (e^{t/\tau_r} - 1)^3 (e^{t(\frac{1}{\tau_r} - \frac{1}{\tau})} - 1)}{\lambda^2 (\tau_r - \tau)(\tau_r + \tau)(\tau_r + 3\tau)[\tau_r(\tau_0 + \tau) + 2\tau_0\tau]}, \quad (\text{H4b})$$

$$\begin{aligned} \langle \Delta x_{A,a}^2 \Delta x_{A,b}^2 \rangle(t) &= T_A^2 \frac{\tau_r^4 (e^{t/\tau_r} - 1)^2 e^{-\frac{4t}{\tau_r} - \frac{t}{\tau}}}{\lambda^2 (\tau_r - \tau_0)(\tau - \tau_r)(\tau_r + \tau)^2 [\tau_r(\tau_0 + \tau) - 2\tau_0\tau][\tau_r(\tau_0 + \tau) + 2\tau_0\tau]} \\ &\times \{ 4\tau_0^4 (\tau - \tau_r)(\tau_r + \tau) e^{\frac{2t}{\tau_r} - \frac{t}{\tau_0}} + (\tau_r - \tau_0)(\tau - \tau_r) [\tau_r^2 (\tau_0 + \tau)^2 - 4\tau_0^2 \tau^2] e^{t(\frac{2}{\tau_r} + \frac{1}{\tau})} \\ &+ (\tau_0 - \tau_r)(\tau_0 + \tau)(\tau_r + \tau) e^{t/\tau} [4\tau_0^2 \tau - \tau_r^2 (\tau_0 + \tau)] \\ &- 2(\tau_0 + \tau) e^{t/\tau_r} [2\tau_0^2 \tau_r + \tau(\tau_0 - \tau_r)(2\tau_0 + \tau_r)] [2\tau_0\tau - \tau_r(\tau_0 + \tau)] \}, \end{aligned} \quad (\text{H4c})$$

$$\begin{aligned} \langle \Delta x_{A,a} \Delta x_{A,b}^3 \rangle(t) &= -T_A^2 \frac{3\tau_r^4 e^{-\frac{4t}{\tau_r}} (e^{t/\tau_r} - 1)}{\lambda^2 \tau (\tau_r + \tau)} \left\{ \frac{\tau^2 (2\tau_0 - \tau_r)(\tau_0 + \tau)}{(\tau_r - 3\tau)(\tau_r - \tau)[\tau_0(\tau_r - 2\tau) + \tau_r\tau]} + \frac{2\tau_0^4 e^{-t(\frac{1}{\tau_0} - \frac{2}{\tau_r} + \frac{1}{\tau})}}{(\tau_0 - \tau_r)(\tau_0 + \tau_r)[\tau_r(\tau_0 + \tau) - 2\tau_0\tau]} \right. \\ &\left. + \frac{(\tau_0 + \tau)[\tau_0(\tau_r + \tau) - \tau_r\tau] e^{t(\frac{1}{\tau_r} - \frac{1}{\tau})}}{(\tau_r - \tau_0)(\tau_r^2 - \tau^2)} + \frac{(\tau_0 + \tau)[\tau(\tau_0 + \tau_r) - \tau_0\tau_r] e^{\frac{3t}{\tau_r} - \frac{t}{\tau}}}{(\tau_0 + \tau_r)(\tau_r^2 - 4\tau_r\tau + 3\tau^2)} + \frac{\tau^2 e^{\frac{2t}{\tau}}}{\tau_r^2 - \tau^2} \right\}, \end{aligned} \quad (\text{H4d})$$

$$\begin{aligned}
\langle \Delta x_{A,b}^4 \rangle(t) = T_A^2 \frac{3\tau_r^4 e^{-\frac{4t}{\tau_r}}}{\lambda^2 \tau (\tau_r + \tau)} & \left\{ - \frac{\tau(2\tau_0 - \tau_r)(\tau_0 + \tau)(\tau_r + \tau)}{(\tau_r - 3\tau)(\tau_r - \tau)[\tau_0(\tau_r - 2\tau) + \tau_r \tau]} \right. \\
& + \frac{8\tau_0^5 (\tau_r + \tau) e^{t(-\frac{1}{\tau_0} + \frac{2}{\tau_r} - \frac{1}{\tau})}}{(\tau_r - \tau_0)(\tau_0 + \tau_r)[\tau_r(\tau_0 + \tau) - 2\tau_0 \tau] \tau_r(\tau_0 + \tau) + 2\tau_0 \tau} - \frac{4(\tau_0 + \tau)[\tau(\tau_0 + \tau_r) - \tau_0 \tau_r] e^{\frac{3t}{\tau_r} - \frac{t}{\tau}}}{(\tau_0 + \tau_r)(\tau_r^2 - 4\tau_r \tau + 3\tau^2)} \\
& \left. + \frac{4(\tau_0 + \tau)[\tau_0(\tau_r + \tau) - \tau_r \tau] e^{t(\frac{1}{\tau_r} - \frac{1}{\tau})}}{(\tau_0 - \tau_r)(\tau_r - \tau)(\tau_r + 3\tau)} + \frac{\tau(2\tau_0 + \tau_r)(\tau_0 + \tau) e^{\frac{4t}{\tau_r}}}{(\tau_r + 3\tau)[\tau_r(\tau_0 + \tau) + 2\tau_0 \tau]} + \frac{2\tau e^{\frac{2t}{\tau_r}}}{\tau - \tau_r} \right\}, \quad (\text{H4e})
\end{aligned}$$

from which we deduce

$$\langle \Delta x_A^4 \rangle = \langle \Delta x_{A,a}^4 \rangle + 3\langle \Delta x_{A,a}^4 \Delta x_{A,b} \rangle + 6\langle \Delta x_{A,a}^2 \Delta x_{A,b}^2 \rangle + 3\langle \Delta x_{A,a} \Delta x_{A,b}^3 \rangle + \langle \Delta x_{A,b}^4 \rangle. \quad (\text{H5})$$

-
- [1] T. Toyota *et al.*, *Soft Matter* **7**, 3234 (2011).
- [2] D. Mizuno, C. Tardin, C. F. Schmidt, and F. C. MacKintosh, *Science* **315**, 370 (2007).
- [3] N. Fakhri, A. D. Wessel, C. Willms, M. Pasquali, D. R. Klopfenstein, F. C. MacKintosh, and C. F. Schmidt, *Science* **344**, 1031 (2014).
- [4] B. Stuhmann, M. Soares e Silva, M. Depken, F. C. MacKintosh, and G. H. Koenderink, *Phys. Rev. E* **86**, 020901(R) (2012).
- [5] A. Caspi, R. Granek, and M. Elbaum, *Phys. Rev. E* **66**, 011916 (2002).
- [6] P. Bursac *et al.*, *Biochem. Biophys. Res. Comm.* **355**, 324 (2007).
- [7] W. W. Ahmed, É. Fodor, and T. Betz, *Biochimica et Biophysica Acta (BBA)-Molecular Cell Research* (2015), doi: 10.1016/j.bbamcr.2015.05.022.
- [8] M. Soares e Silva, B. Stuhmann, T. Betz, and G. H. Koenderink, *New J. Phys.* **16**, 075010 (2014).
- [9] C. Storm, J. J. Pastore, F. C. MacKintosh, T. C. Lubensky, and P. A. Janmey, *Nature (London)* **435**, 191 (2005).
- [10] M. Annunziato, *Phys Rev E* **65**, 021113 (2002).
- [11] E. Ben-Isaac, YongKeun Park, G. Popescu, F. L. H. Brown, N. S. Gov, and Y. Shokef, *Phys. Rev. Lett.* **106**, 238103 (2011).
- [12] A. Ghosh and N. S. Gov, *Biophys. J.* **107**, 1065 (2014).
- [13] A. Rahman, *Phys. Rev.* **136**, A405 (1964).
- [14] P. Bursac, G. Lenormand, B. Fabry, M. Oliver, D. A. Weitz, V. Viasnoff, J. P. Butler, and J. J. Fredberg, *Nature Materials* **4**, 557 (2005).
- [15] N. Gal, D. Lechtman-Goldstein, and D. Weihs, *Rheologica Acta* **52**, 425 (2013).
- [16] J. Howard, *Mechanics of Motor Proteins and the Cytoskeleton* (Sinauer Associates, Sunderland, MA, 2001).
- [17] D. Bi, J. H. Lopez, J. M. Schwarz, and M. L. Manning, *Soft Matter* **10**, 1885 (2014).
- [18] F. Backouche, L. Haviv, D. Groswasser, and A. Bernheim-Groswasser, *Phys. Biol.* **3**, 264 (2006).
- [19] S. Khler, V. Schaller, and A. R. Bausch, *Nature Materials* **10**, 462 (2011).
- [20] M. Soares e Silva, M. Depken, B. Stuhmann, M. Korsten, F. C. MacKintosh, and G. H. Koenderink, *Proc. Natl. Acad. Sci. USA* **108**, 9408 (2011).
- [21] O. J. N. Bertrand, D. K. Fygenson, and O. A. Saleh, *Proc. Natl. Acad. Sci. USA* **109**, 17342 (2012).
- [22] É Fodor *et al.*, *Europhys. Lett.* **110**, 48005 (2015).
- [23] É. Fodor, K. Kanazawa, H. Hayakawa, P. Visco, and F. van Wijland, *Phys. Rev. E* **90**, 042724 (2014).
- [24] M. Sheinman, A. Sharma, J. Alvarado, G. H. Koenderink, and F. C. MacKintosh, *Phys. Rev. Lett.* **114**, 098104 (2015).
- [25] C. Wilhelm, *Phys. Rev. Lett.* **101**, 028101 (2008).
- [26] F. Gallet, D. Arcizet, P. Bohec, and A. Richert, *Soft Matter* **5**, 2947 (2009).